Int J Heat Mass Transfer Vol 33 No 11 pp 2439–2449 1990
Printed in Great Britain

0017–9310/90 $3.00 + 0.00

Holographic interferometry applied to rib-roughness heat transfer in turbulent flow

J F LOCKETT† and M. W COLLINS
Thermo-Fluids Engineering Research Centre, The City University, London EC1V 0HB, U K

(*Received* 10 *March* 1989 *and in final form October* 1989)

Abstract—The non-invasive optical method of holographic interferometry is applied to the problem of heat transfer in turbulent flow over square and rounded rib-roughness elements. Besides giving two-dimensional fluid isotherms, it is demonstrated that this method results in reliable local surface heat transfer data. These data are compared with those from alternative experimental methods. While the geometry specifically simulates that on the Advanced Gas Cooled Reactor fuel elements, the results are of general interest, since the rib pitch to height ratio is 7.2:1.

INTRODUCTION

HOLOGRAPHIC interferometry represents the combination of classical interferometry with the recent development of a source of highly coherent light, namely, the laser. The method, and its differing techniques, have been applied in various branches of engineering, and its historical development and the current literature with particular reference to heat transfer have been reviewed in ref. [1]. It was successfully applied some years ago by Walklate [2] to the problem of heat transfer by forced convection from a smooth plate to a turbulent boundary layer. In this application, the interferometric fringes are essentially isotherms. In reporting his work, Walklate explained the interferometric theory and basic holographic method, together with an analysis of the maximum resolution possible of the non-dimensional cross-stream coordinate Δy^+. Convincing quantitative data were presented in terms of local Nu as a function of Re, and fluid temperatures non-dimensionalized as a $T^+ - t^+$ plot. Hence this method represents a novel approach to providing data for both engineering performance and the thermal boundary layer.

Its potential, however, is far more than this, since it can be extended in various important ways. Firstly, more complex surface geometries can be treated. In fact, Walklate applied it to a rectangular rib-roughness, where a single interferogram usefully encompassed both two ribs, and the inter-rib gap [3]. Secondly, by using the holographic method in a 'real-time' mode, the movement of the thermal eddies in the far wall region may be recorded. This gives a novel approach to flow visualization, since there the temperature (via enthalpy) is a 'passive scalar' and hence the fluid eddy behaviour is given. However, and more importantly, since the data are quantitative, the method provides an experimental comparison with the time-dependent effects and fluid-thermal field relationships, of predictive methods such as LES, large eddy simulation (for example, Grotzbach [4]). Finally, the use of lasers in interferometry provides the possibility of investigating three-dimensional effects. As applied by Walklate, the wind tunnel was designed to minimize spanwise effects, and the laser beams crossed the flow in this direction. Hence the record obtained was a two-dimensional spanwise-averaged interferogram. Bryanston-Cross *et al* [5], in the corresponding high-speed compressible flow application, similarly obtained a two-dimensional interferogram the fringes of which were iso-Mach number contours. However, methods are available for recording three-dimensional effects, and then using tomography to reconstruct the full three-dimensional field [6].

Hence, holographic interferometry provides a method which is optical, non-invasive and whole-field in character, and here can investigate thermal effects. In principle, it may be used in conjunction with seeded fluid flow field methods, such as the two-dimensional PIV (particle image velocimetry [7]) or the three-dimensional HCV (holocinematographic velocimetry [8]). This means it would be possible to obtain simultaneous whole-field real-time fluid and thermal data, truly comparative with sampled data from current computational fluid dynamics codes. In fact, as with them, the sheer quantity of data obtained is so large that automatic processing and methods of sampling become paramount needs. With care, such methods could accommodate either experimental or predictive data, and the rather exciting prospect opens up of being able to carry out coherent structure investigations by either means. For a comprehensive review of the approach to coherent structure studies in turbulence see Hussain [9], although the possibilities described here are not developed.

†Now at British Gas plc, Research & Technology Division, Midlands Research Station, Solihull, W Midlands, B91 2JW, U K

NOMENCLATURE

C_{fr}	correction factor
C_p	specific heat
D	distance along heated surface
D_e	equivalent duct diameter (4 × cross-sectional area) (wetted perimeter)
e	rib height
e^+	non-dimensional rib height, $e\sqrt{(\tau_w/\rho)}/\nu$
G	Gladstone–Dale constant, 2.25×10^{-4} m^3 kg^{-1}
H	channel height
k	thermal conductivity
n	refractive index
N	fringe order
Nu_l	local Nusselt number, $D_e(\mathrm{d}T/\mathrm{d}y)_{y=0}/(T_w-T_B)$
Nu_m	average Nusselt number, $(1/D)\int_0^D Nu_l\,\mathrm{d}l$
Pr	Prandtl number, $C_p\mu/k$
q_w	wall heat flux
Re	Reynolds number, D_eU_B/ν
S	pitch length
St	Stanton number
T	absolute temperature
T_B	bulk temperature
T_i	temperature of ith fringe
T_r	reference temperature
T_w	wall temperature
T^-	non-dimensional temperature, $(T_w-T)\rho C_p\sqrt{(\tau_w/\rho)}/q_w$
U_B	bulk velocity
W'	optical width of the working section
x	coordinate of undisturbed ray path
y	wall normal displacement
y^+	non-dimensional normal displacement $y\sqrt{(\tau_w/\rho)}/\nu$

Greek symbols

λ	wavelength of light
μ	dynamic viscosity
ν	kinematic viscosity
ρ	density
ρ_r	reference density
τ_w	wall shear stress
ϕ	ray path within working fluid

A programme of work with the general aims as expressed above is being developed from the original success of Walklate. We have been able to apply holographic interferometry to forced convection heat transfer from roughness elements as reported here. Also, we have successfully developed several real-time methods [10, 11]. Fringe and data processing software has also been developed [12–14]. In conjunction with Dr P. Ereaut of A.E.R.E. Harwell, it has been initially demonstrated that PIV can be carried out simultaneously. It is intended to investigate this more thoroughly. Also, a comparison of temperature measurement with LES predictions has been made in collaboration with Prof. D. C. Leslie and the Turbulence Unit at Queen Mary College, London [15]. Finally, we have made assessments of the problems of three-dimensional investigations with tomographical reconstructions [16], and of unifying the data handling of experimental and predictive methods [17].

This paper reports a detailed study of two problems of roughness element heat transfer. While the geometry simulates as closely as possible the nominal conditions on the Advanced Gas Cooled Reactor fuel element, the results are of general interest, since the rib pitch to height ratio is 7.2:1. In his work, Walklate [3] encountered some negative local heat transfer rates and attributed this to an incorrect solid-to-gas conductivity ratio. By careful choice of the metal base, we were able to simulate the ratio much more closely, and did not encounter the problem.

The major obstacle to overcome when using interferometry to study rib-roughness geometries is the varying degree of refraction encountered around the rib. This means that there is no one definite plane that can be focused to make refraction errors negligible. To overcome this, wall shear velocities are used to obtain the height of the boundary layer, in non-dimensional units, which then enables the observed fringe field to be extrapolated to the wall. In this manner detailed quantitative heat transfer data can be achieved for the entire rib surface. If wall shear velocities are not available, then only qualitative distributions are obtainable. Both quantitative and qualitative results are reported here.

ALTERNATIVE METHODS FOR STUDYING RIB-ROUGHNESS HEAT TRANSFER

Other experimental techniques previously applied to the study of rib-roughness geometries are

(i) thin film naphthalene,
(ii) evaporation from water absorbent paper,
(iii) electro-chemical technique,
(iv) copper foil.

(i) *Naphthalene.* Utilizing the heat/mass transfer analogy, the heat transfer may be determined by measuring the mass transfer from the surface of a volatile solid. An ideal substance is naphthalene. Kattchee and Mackiewicz [18] coated a metal surface with naphthalene and measured the amount removed after a predetermined period of flow exposure. Their results are illustrated in Fig. 7 and show the heat transfer distribution to vary significantly around the rib. Using

their technique, absolute values could not be determined, but from the distribution obtained, estimates of the maximum surface temperature could be achieved

(ii) *Evaporation from water absorbent paper.* Another mass transfer analogy technique, developed by Williams and Watts [19] involves measuring the evaporation rate of water from cobaltous chloride impregnated paper At the start of a test water is sprayed evenly over the paper's surface and it is then placed in a wind tunnel The time required for the chloride paper to turn from pink to blue is proportional to the heat transfer coefficient Absolute values cannot be determined but the distribution is again illustrated in Fig 7

(iii) *Electrochemical technique* The transfer rate of certain ions in aqueous solutions to an electrode is measured and is directly proportional to the heat transfer rate Berger and Hau [20] employed an aqueous solution of potassium ferri- and ferro-cyanide with sodium hydroxide as an inert electrolyte. A strip of nickel was the anode and a ribbed surface of nickel the cathode. The electric current at certain stations around the surface is then recorded and this enables the heat transfer distribution to be determined. These results of Berger *et al* are for a rib spacing of 7 :1 and so are not directly comparable but similar trends are achieved, as in Fig 7

(iv) *Copper foil analysis* Known currents are passed through copper strips placed on a ribbed surface and the power dissipated by each strip is determined from the voltage drop across the strip. If the resistance of the strip is known the temperature may be determined and then an average heat transfer coefficient for the strip may be calculated. The results for the square ribbed surface [21] are illustrated in Fig 7 and a good agreement with the previous results is observed

Of the techniques discussed above only the copper foil method can give absolute values for the heat transfer coefficient But this technique is experimentally demanding and individual surfaces have to be fabricated from copper for the tests to proceed In addition only coarse measurements may be undertaken because of a limit on the width of the copper foil for instrumentation purposes

Of the four methods used previously to study the heat transfer distribution, therefore, only one was able to give absolute values and none could give information concerning the flow field Adequate resolution was also limited in the above techniques However, by employing the new method of holographic interferometry, not only surface heat transfer coefficients, but also the fluid thermal field may be measured In all regions except close to the heated surface, this is convection dominated, and closely related to the flow field In fact, if the method is applied in 'real-time', the behaviour of thermal eddies may be traced, thus representing a new method of investigating the flow eddy structure

EXPERIMENTAL APPARATUS

A wind tunnel with an aspect ratio of 4 1 and an equivalent diameter (D_e) of 0 12 m was used throughout the investigation A centrifugal flow fan provided the air flow, and using the diffuser, plenum, rounded entry and flow entry section of [$20 \times D_e$] (all shown in Fig 1(a)), a 'square' and symmetrical velocity profile was achieved in both (perpendicular) cross-sections of the duct.† An exit section of [$3\,9 \times D_e$] removed any downstream effects from the working section All interferograms were taken [$24 \times D_e$] from the inlet through the glass walls of this section. Heating was provided by eight electrical pad resistance heaters Conduction in the AGR fuel element cladding is an important effect, modelled well by this method, but not by the 'surface effect' techniques of the alternative approaches. Ribs at a spacing S/e of 7 2 1 (Fig 1(b)) were attached along the entire base of the tunnel to ensure a fully-developed flow field existed

As already discussed, most work in the past has been on square-section ribs, as depicted in Figs. 1(b) and 3 Not only was this the nominal AGR geometry, but also the optimized 'standard-case' pitch to height ratio geometry. However, a rounded rib profile illustrated in Fig 8 was also investigated, this being much more typical of the actual AGR geometry The ribbed surface was machined from a solid block of stainless steel to ensure thermal continuity between the base of the heated section and the ribs.

A fairly standard optical circuit was used for the interferometer, consisting of shutter, beam-splitter, beam expanders, Schlieren mirrors, plane mirrors, and lens (see Fig. 2) The laser was a 3 W argon-ion Spectra-Physics model, the high power being required for subsequent real-time work This successful and novel application has been partially reported in ref [10] already with more conclusive experience to be published [11].

APPLICATION OF INTERFEROMETRIC THEORY

When two beams of coherent light fall upon a light sensitive material an interference pattern results. Once the material has been developed a diffraction grating is formed that is able to diffract light from one of the original light beams to form a reconstructed image of the remaining original beam. This technique of forming a diffraction grating (hologram) is the basis of holographic interferometry. In the particular method used here, known as double exposure, the holographic image is recorded on two occasions on the same light sensitive material Any variation in the phase of the light passing through the object between exposures results in a set of fringes superimposed over

† This was in the initial plane-channel (that is, unribbed) test work

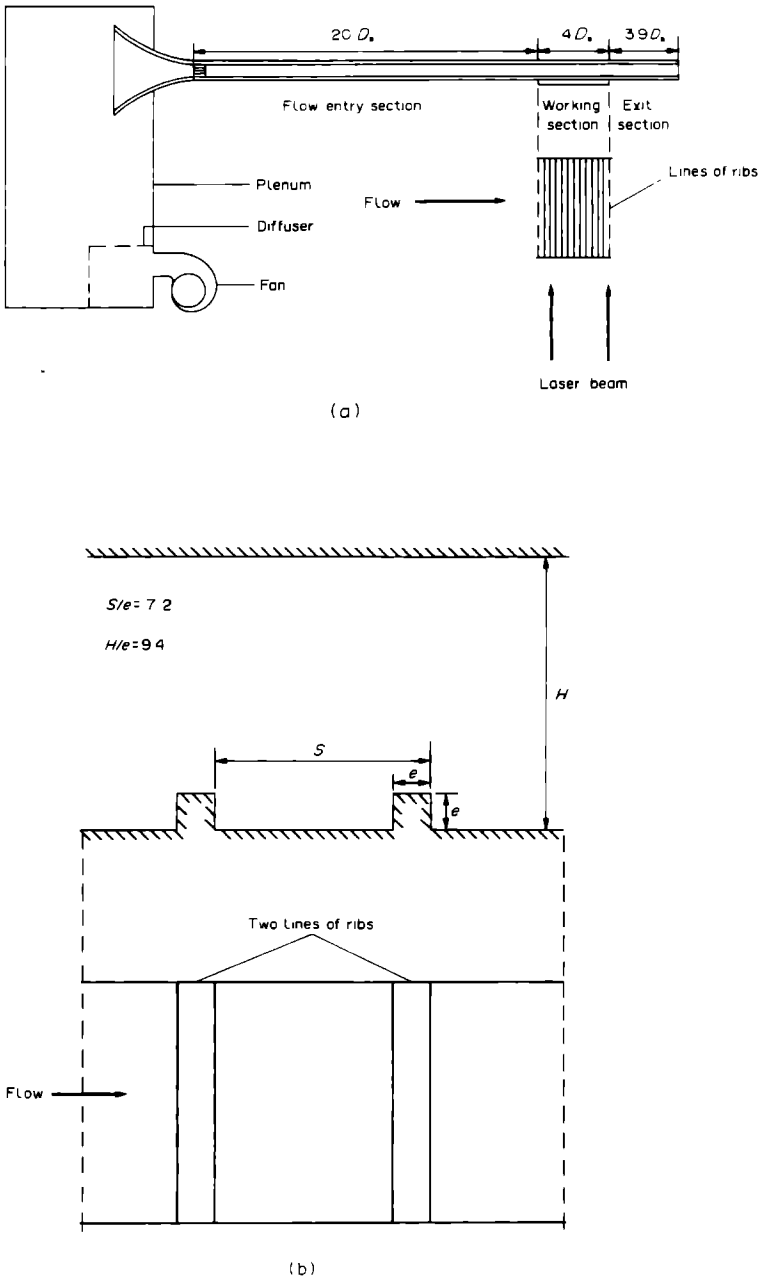

FIG 1 Wind tunnel and rib-roughened heated section (a) schematic diagram of wind tunnel, (b) square-rib geometry studied

the image that can be directly related to the degree of phase distortion In this manner the temperature field over a two-dimensional plane surface may be determined according to the following theory

To analyse the interferogram the equation of interferometry given by Hauf and Grigull [22] for an incompressible two-dimensional boundary layer is used This gives

$$T_i = T_r\left[1 - \frac{N\lambda C_{ll}}{G\rho_r W}\right] \tag{1}$$

where C_{ll} is a correction factor that allows for the deviation due to refraction of the ray path from the ideal path parallel to the surface. It is given by

$$C_{ll} = W\left[T_{\phi=0}\int_{\phi}\frac{\mathrm{d}\phi}{T_\phi}\right]^{-1}_{i-1} \tag{2}$$

where the ray path ϕ is traced using refraction theory as below

$$\frac{\mathrm{d}^2y}{\mathrm{d}x^2} = \frac{1}{n}\frac{\mathrm{d}n}{\mathrm{d}y} = \left[\frac{-G\rho_r}{(T_i T_r + G\rho_r)T}\right]\frac{\mathrm{d}T}{\mathrm{d}y} \tag{3}$$

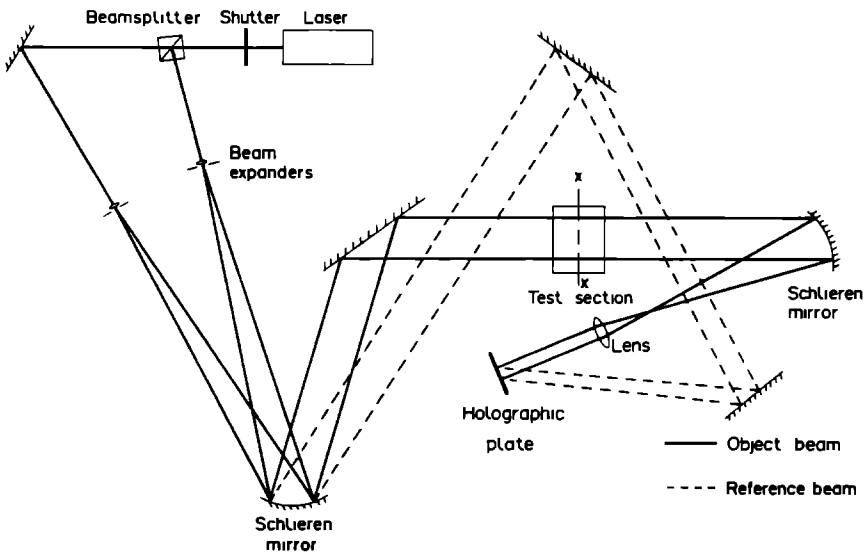

FIG 2 Optical diagram of image-plane interferometer

Using a Taylor series expansion, and taking Δx small compared with W

$$\left.\frac{dy}{dx}\right|_{x+\Delta x} = \left.\frac{dy}{dx}\right|_{x} + \Delta x \left.\frac{d^2y}{dx^2}\right|_{x} \tag{4}$$

and

$$y|_{x+\Delta x} = y|_{x} + \Delta x \left.\frac{dy}{dx}\right|_{x} + \tfrac{1}{2}\Delta x^2 \left.\frac{d^2y}{dx^2}\right|_{x}. \tag{5}$$

Initially, C_{ij} is set to unity, and the ray path traced using the boundary conditions

$$\left.\frac{dy}{dx}\right|_{x=0} = 0$$

(that is, ray enters parallel to wall) and

$$y|_{x=0}$$

is the measured displacement from the wall

Consecutive iterations are performed until C_{ij} becomes constant Then the temperature field given by equation (1) can be determined provided that the refraction effect does not result in ray crossing With the known ambient temperature being assigned to T_r, quantitative values T_i are obtained for each fringe of order N In fact, for our work a fringe-to-fringe temperature difference of 2 K results. This means a total of around 15 fringes is used to avoid buoyancy effects. In fact, at the lowest Re and this temperature difference of 30 K, the relevant dimensionless group of Richardson number had a value of 1.5×10^{-2} We estimated the resultant error in Nu to be only $\pm 0.3\%$, but negligible at high Re [25]

The fringes are close together and narrow near the wall, but broader in the main flow. Two factors can cause loss of clarity, firstly, temperature changes during the exposure time of the second exposure, and secondly, changes due to spanwise turbulence effects over the ray path The high power of the laser (3 W nominal) meant that exposure times were limited by the camera, not the illumination In fact, in all our experience, time effects in this context were not significant † However, spanwise structures did affect the fringes by blurring the edges of the broadest ones furthest from the wall Hence, the method accommodates the spanwise problem rather well, leading to sharp and narrow near-wall fringes (which are closely-spaced, and therefore subject to the ray crossing problem), and diffuse broad far-wall fringes, where ray crossing is not such a problem Hence, the near-wall temperature gradient is accurately obtainable (and therefore the wall heat flux) and this is then extrapolated to give the wall temperature difference relative to the zero-order fringe furthest from the wall Since the known ambient temperature is assigned to this fringe, the actual wall temperature is known, this giving the local Nu

Hence the two-dimensional (spanwise averaged) temperature field in the fluid, and the local wall temperature and Nu are all quantitatively obtainable.

DISCUSSION OF RESULTS

Square-rib geometry

A typical double exposure interferogram taken of the thermal field is shown in Fig. 3 for $Re = 10\,800$ Measurements were in fact taken for Re varying from 10 000 to 30 000, for which the non-dimensional rib height e^+ ranged from 95 to 285. At this stage, no special focusing was undertaken, and this meant that clear images were unobtainable for $Re > 30\,000$.

Analysis of the interferograms yields the absolute heat transfer distribution shown in Fig 4 From this

† This is consistent with Walklate's observations [2]

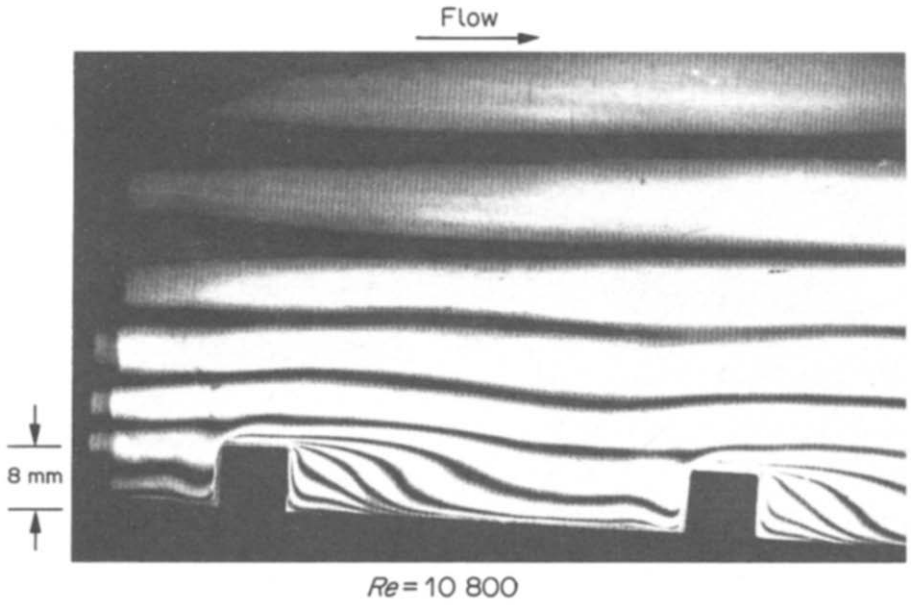

Fig 3 Typical double exposure image—square-rib geometry

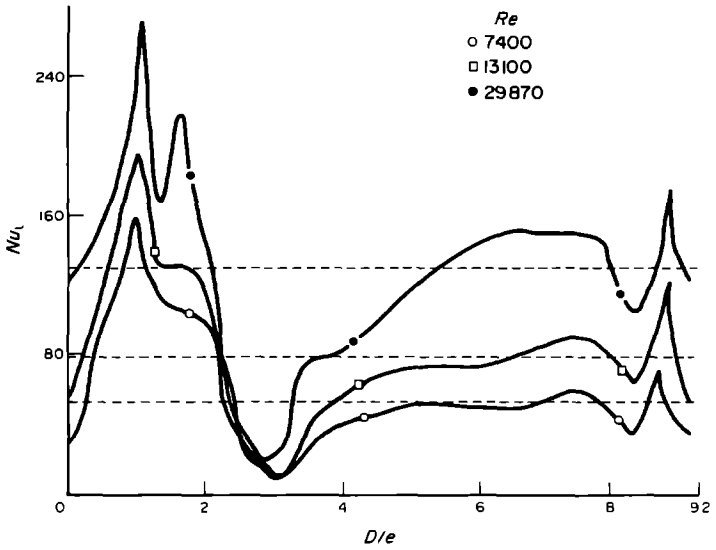

Fig 4 Absolute Nusselt number distribution for square-rib geometry

an average Nusselt number may be calculated for each value of *Re*. A comparison of this data with corresponding smooth surface results (i.e heated section with no ribs) is shown in Table 1 The gain decreases with increasing *Re* While this is to be expected, the extent of the decrease is rather too large

Table 1 Comparison of average heat transfer coefficient–square-rib geometry with smooth channel

Reynolds number	Nusselt number, Nu_{av} Smooth	Square rib-roughened	Gain
7400	25	56	2 24
13 100	39 4	79 5	2 01
29 870	76 1	128	1 68

This may be due to resolution errors being larger at higher flow rates, which makes the determination of the wall position increasingly less certain. Any error here is correspondingly reflected in the calculation of *Nu*

The Stanton number may then be obtained and results are compared in Fig 5 with the data of Watts and Williams [21] and of Warburton [23]. Since their definitions of *Re* were not the same, and could not be made consistent with that used here, the comparison is not as reliable as it might be Despite this, there is, in fact, reasonable agreement, particularly if a different extrapolation is used instead of that estimated by Watts and Williams [21] Unfortunately, no specific low *Re* data could be found to clarify the extrapolation.

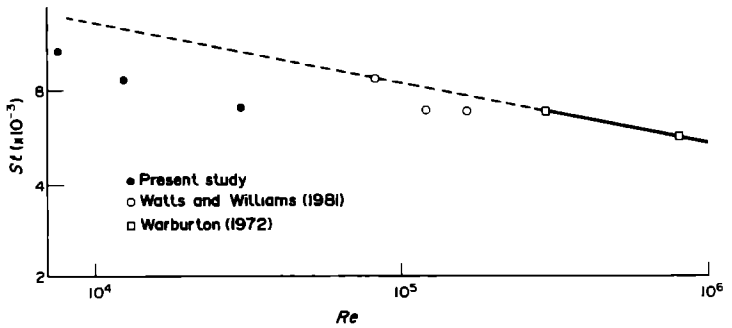

FIG 5 Variation of Stanton number with Reynolds number for square ribs—comparison with published data

To facilitate comparison of each Reynolds number plot, all are normalized by the average *Nu* for the surface, the resulting plot is shown in Fig 6 with published data of other authors in Fig. 7 The distribution comprises four regions, with a brief description of each being given below.

(i) *Forward facing rib wall* ($0 < D/e < 1$) An increasing heat transfer coefficient is apparent from the base to the tip of the rib Refraction effects are severe in this region, because the recirculation region is relatively small and the boundary layer is thin.

(ii) *Rib top* ($1 < D/e < 2$) The maximum heat transfer for the entire geometry occurs at the leading edge of the rib tip The heat transfer then decreases and increases again which is indicative of a recirculation region (i e. thickening and then thinning of the boundary layer) on the rib top. This effect (see also Fig 4) is *Re*-dependent, being absent at 7400 and most pronounced at 30 000 At the latter *Re*, the forward facing recirculation has grown in size until it reaches the same height as the rib These conditions would then be favourable for a recirculation region to form on the top of the rib, immediately past the sharp leading corner

(iii) *Rear facing rib wall* ($2 < D/e < 3$). A dramatic decrease in heat transfer occurs because the trailing edge recirculation zone is entered Broad and widely spaced fringes are observed. However, this region does not suffer from refraction effects and so the wall position is easily located, which aids in assessing the wall location in the other regions.

(iv) *Inter-rib region* ($3 < D/e < 9.2$) This is by far the largest region for heat transfer and yet it does not yield a proportionate amount (The rib, for its size, is the better region) A peak in heat transfer occurs at $0\ 35e$ in front of the rib, which agrees well with Walklate's [3] value of $0\ 4e$, for the entire Reynolds number range A similar peak is given by the copper foil technique of Watts and Williams [21] but the naphthalene results give a peak of $0\ 7e$ in front of the rib while the other methods failed to identify it The error for the naphthalene result could be explained by the change in the surface geometry as the test progressed The turbulence intensities and shear stress measurements of Lawn [24] display a similar peak An explanation for this phenomenon is that the flow around the forward facing rib face is convected to the inter-rib region by the primary recirculation A

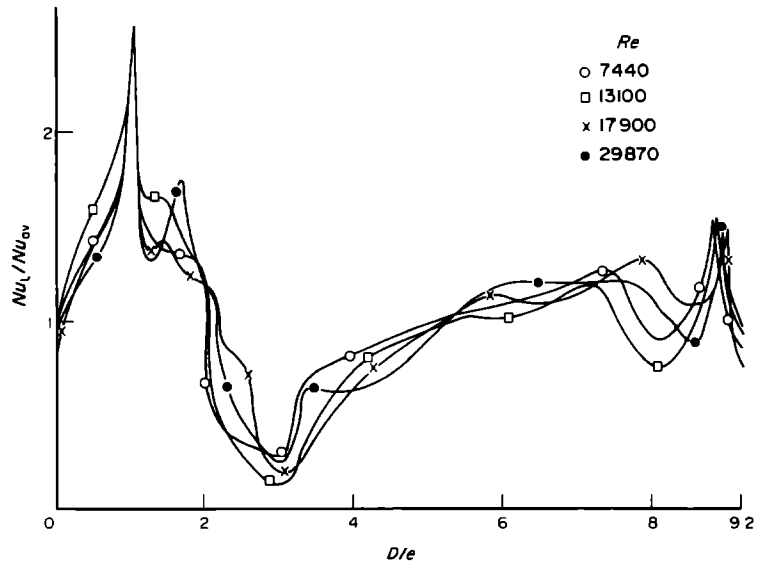

FIG 6 Normalized Nusselt number distribution for square-rib geometry—authors' results

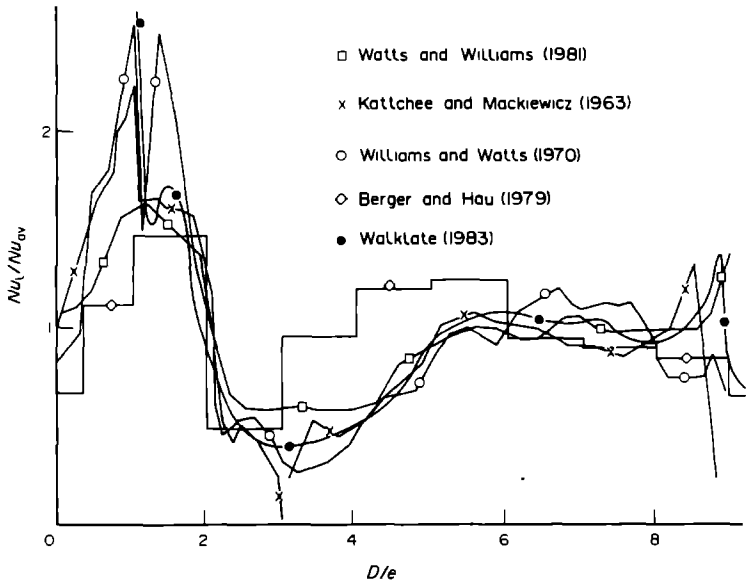

FIG 7 Normalized Nusselt number distribution for square-rib geometry—published data

secondary recirculation in the corner is caused by separation of this flow At the point of reattachment a high heat transfer rate is observed.

Another peak in heat transfer, lower than the first one, is observed in the inter-rib region It is not, as one might expect, at the reattachment point of the trailing recirculation region, but is displaced towards the trailing rib. Two effects are combining here. The boundary layer is growing after reattachment and so one would expect the heat transfer rate to fall. However, this effect is opposed by faster moving fluid approaching the wall after it has passed over the rib top Hence the heat transfer continues to increase until the second peak occurs nearer to the trailing rib Its exact location is Reynolds number dependent and so cannot be identified precisely

Rounded-rib geometry

A typical double exposure interferogram for the rounded-rib geometry is shown in Fig 8 for $Re = 7330$ ($e^+ = 70$) Measurements were taken over a range of Re from this value to 53900 (up to $e^+ = 602$) By the addition of a focusing lens reactor rib Re could be achieved Unfortunately no data are available for the momentum field over this geometry and this meant that the turbulent boundary layer extrapolation procedure (i e. knowing y^+ values for a given distance from the wall) was not feasible Hence, only normalized heat transfer data could be determined, as described below (See Appendix for more details)

Firstly, the fringe spacing was determined up to the ray crossing regime The temperature gradient at this location was then used to assess the local Nusselt number by assuming that the ray crossing error is consistent around the geometry This is a reasonable assumption given that there are no sharp corners for the flow to encounter However, this technique will enhance the heat transfer in the recirculation region relative to the rest of the geometry. But as the heat transfer rate is poor in this area, the relative increase will have a minor effect on the distribution

The normalized Nusselt number distribution for the rounded-rib geometry is shown in Fig. 9 with no available published work for comparison Immediately apparent is a Reynolds number dependency at the rear of the rib. This arises because the rounded geometry is more 'streamlined' and so enables the reattachment condition to vary widely with flow rate There are no sharp corners to dictate where flow separation occurs and hence it is flow rate dependent Peak heat transfer still occurs at the leading edge of the rib top and the distribution in the inter-rib region is similar to that of the square-rib geometry. For this geometry, therefore, the rib is discussed as one entity followed by a description of the inter-rib region heat transfer

(i) *Rounded rib* ($0 < D/e < 3\,43$) The sharp peak heat transfer at the leading edge of the square rib has disappeared for a more gradual variation in heat transfer This is particularly apparent for the low Reynolds number flows. The sharp decrease in heat transfer at the rear of the rib top has also disappeared to be replaced by a more gradual change. This is not so obvious for low flow rates but for higher flows there is no distinguishable position where a fall in heat transfer occurs Trailing edge recirculation regions are driven relatively faster by the main flow so that an appreciable amount of heat is transferred down the rear facing wall Also, the bottom of the rib is now a curved surface and this prevents a region of slow moving fluid forming. An increased heat transfer down this face is therefore observed

No recirculation regions were apparent over the rib

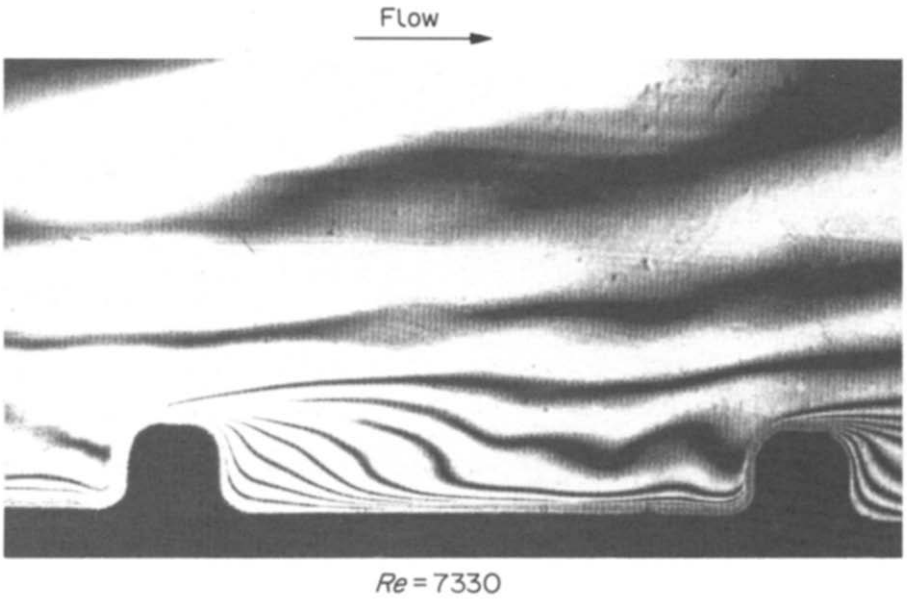

FIG. 8 Typical double exposure image rounded-rib geometry

top, even at flow rates of $Re \approx 30\,000$ where they are most likely to occur Hence, if a separation region does occur it is very small.

(ii) *Inter-rib region* ($3.43 < D/e < 8\,55$) For this geometry no peak in heat transfer was detected just prior to the forward facing rib wall. At low flow rates a fall and rise were observed but no peak. Reattachment of the trailing edge recirculation varies depending upon the Reynolds number The higher the flow rate the closer the reattachment is to the trailing rib face Also, a more uniform heat transfer region is observed after reattachment. The flow approaching the wall after passing over the rib is not as strong for this geometry because the rib is more streamlined As a result the peak in heat transfer for the region occurs further from the rib. For example, at a Reynolds number of 53 000 ($e^+ = 602$) a relatively constant heat transfer region is observed from $3.5e$ to $0\,5e$ prior to the rib face, with a peak occurring at $1\,25e$ before the rib This illustrates the reduced effect of the flow approaching the wall.

Estimate of experimental error

Although not presented here, the basic fluid measurements of mean velocity and pressure were subject to estimated errors of around $\pm 1\%$, with the exception of use of a Preston tube with a total error of $\pm 4.6\%$

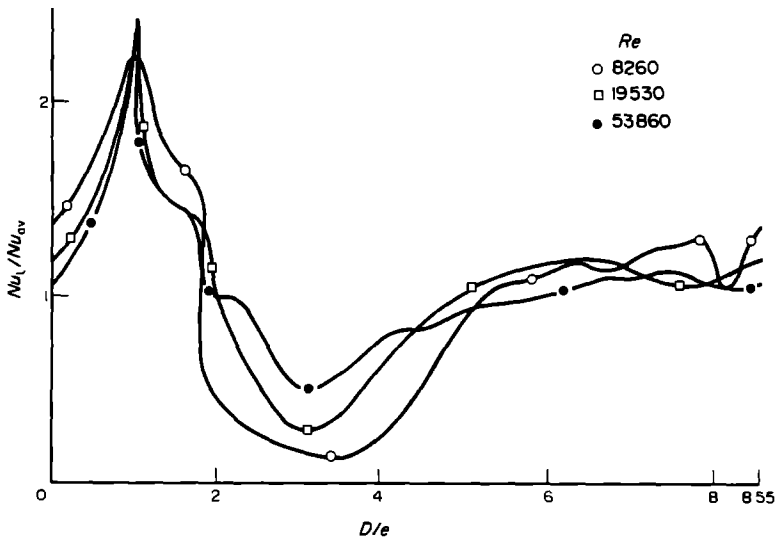

FIG. 9 Normalized Nusselt number distribution for rounded-rib geometry.

What is of immediate interest is the estimate for heat transfer errors and this is carefully studied in ref [25], Appendix B Two broad sources arise, due to the method and instrumentation, and due to the measurements themselves. They comprise (1) refraction effects, (2) diffraction effects, (3) end effects, (4) buoyancy, (5) resolution, (6) stray thermal currents, (7) emulsion shrinkage and (8) optics misalignment.

These were all estimated at low and high Reynolds numbers and the only values above 1% were due to refraction at high *Re* (4.7%), end effects at low *Re* (1 9%), and resolution of fringes (4 7%) The combined error margin was assessed as 5.2% (low *Re*) and 6 7% (high *Re*). However, it should be noted that the common resolution uncertainty, (5) above, could be improved by automatic fringe analysis.

A final source of error is also due to refraction, which in being optimized by focusing, is lessened in the near wall, but enhanced in the far wall region This field-dependent error is not linear and its location is *Re* dependent. It is estimated at worst to add no more than 2% uncertainty in fringe location, further to those errors above

CONCLUSIONS

In this paper it has been shown that holographic interferometry is a useful diagnostic tool for the engineer to study thermal fields In this study, it has been applied to the investigation of heat transfer distribution and associated hot spots around ribbed geometries, of which one has not been studied previously New information is now available to enable the operating limits of flow over rounded ribs to be established The heat transfer distribution was found to be Reynolds number dependent for the rounded rib, but independent for the square rib This fact is easily observable by viewing the fringes at the rear of the rib Maximum and minimum heat transfer always occurred at the leading edge of the top of the rib, and the base of the rear facing rib wall, respectively

These results illustrate the great advantage of the method, the fringes of which give fluid isotherms, their closeness indicating magnitude of heat transfer rate Both qualitative (thermal structure visualization) and quantitative (temperature and local heat transfer) data are readily available from the same image

The method has subsequently successfully been applied to give real-time information, and the further problem of three-dimensional investigations has been addressed

Acknowledgements—The experimental work described was sponsored via CASE Studentship EA004 by Science and Engineering Research Council and Central Electricity Generating Board, Berkeley Nuclear Laboratories We also gladly acknowledge the advice given in the discussions held with Dr P Walklate

REFERENCES

1 J F Lockett and M W Collins, Holographic interferometry and its applications to turbulent convective heat transfer, *Int J Optical Sensors* 1(3) 191 210 (1986)
2 P J Walklate, A two wavelength holographic technique for the study of two-dimensional thermal boundary layers, *Int J Heat Mass Transfer* **24**, 1051 1057 (1981)
3 P J Walklate, A holographic technique for the study of heat transfer from a rib-roughened surface, *Proc 3rd Int Symp on Flow Visualization*, University of Ann Arbor, p 763 (1983)
4 G Grotzbach, Application of the TURBIT-3 subgrid scale model to scales between large eddy and direct simulations, *Proc Conf Euromech 199, Direct and Large Eddy Simulation of Turbulent Flows* University of Munich, Sept /Oct (1985)
5 P J Bryanston-Cross, T Lang, M L G Oldfield and R J G Norton, Interferometric measurements in a turbine cascade using image-plane holography, *Trans ASME J Engng Pwr* **103**, 124 (1981)
6 W Ostendorf, F. Mayinger and P Mewes, A tomographical method using holographic interferometry for the registration of 3-dimensional unsteady temperature profiles in laminar and turbulent flow, *Proc 8th Int Heat Transfer Conf*, San Francisco, August, Vol 2, pp 519–524 (1986)
7 I Grant and G H Smith, Modern developments in particle image velocimetry, Department of Offshore Engineering, Heriot-Watt University (1987)
8 L M Weinstein, B Beeler and A M Lindemann, High speed holocinematographic velocimeter for studying turbulent flow control physics, Paper AIAA-85-0526, A I A A Shear Flow Control Conf , Boulder, Colorado, March (1985)
9 A K M F Hussain, Coherent structures—reality and myth, *Physics Fluids* **26**, 2816 (1983)
10 J F Lockett and M W Collins, Problems in using holographic interferometry to resolve the four-dimensional character of turbulence Part I theory and experiment, *J Opt Sensors* 1(3), 211–224 (1986)
11 J F Lockett and M W. Collins, Experimental–real time techniques using holographic interferometry for turbulent forced convection, *J Phys D, Appl Phys* , to be submitted
12 J C Hunter and M W Collins, Holographic interferometry and digital fringe processing, *J Phys D, Appl Phys* **20**, 683–691 (1987)
13 J C Hunter and M W Collins, The semi-automatic analysis of compressible flow interferograms, *Meas Sci Technol* **1**, 238–246 (1990)
14 J C Hunter and M W Collins, Typically encountered problems in the automatic analysis of infinite fringe background holographic interferograms, 4th Ann FASIG Mtg, 'Fringe Analysis '89', Loughborough, April (1989)
15 J C Hunter, H M Tsai, J F Lockett, P. R Voke, M W Collins and D C Leslie, A comparison of large eddy simulation predictions of a thermal layer with holographic interferograms, *Proc 5th Int Conf on Numer Meth for Thermal Problems*, Montreal, Canada Pineridge Press, Swansea (1987)
16 J C Hunter and M W Collins, Three-dimensional refractive index field reconstruction from holographic interferograms, *Int J Optoelectronics* **4**(2), 95–132 (1989)
17 A E R E Harwell, Data processing requirements for coherent structures, Contract H2C 849347B (1988)
18 N Kattchee and W V Mackiewicz, Effects of boundary layer turbulent promoters on the local film coefficient of ML 1 fuel elements, *Nucl Sci Engng* **16**, 31–38 (1963)
19 F Williams and J Watts, The development of rough surfaces with improved heat transfer performance and a study of the mechanisms involved, *Proc 4th Int Heat Transfer Conf* , Versailles (1970)
20 F P Berger and K F Hau, Local mass/heat transfer

distribution on surface roughened with small square ribs, *Int J Heat Mass Transfer* **22**, 1645 (1979)
21 J Watts and F Williams, A technique for the measurement of local heat transfer coefficients using copper foil, CEGB Report RD/B/5023/N81, Central Electricity Generating Board (1981)
22 W Hauf and W Grigull, Optical methods in heat transfer, *Adv Heat Transfer* **6**, 133–365 (1970)
23 C Warburton, The results of heat transfer and pressure drop tests in the B N C air rigs on surface roughened by transverse ribs, CEGB Report RD/B/M1956, Central Electricity Generating Board (1972)
24 C J Lawn, Flow measurements for establishing heat transfer, CEGB Report RD/B/N3514, Central Electricity Generating Board (1976)
25 J F Lockett, Heat transfer from roughened surfaces using laser interferometry, Ph D Thesis, Dept of Mech Engng, City University, London (1987)
26 A E R E Harwell, Private communication (1987)

APPENDIX QUANTITATIVE DETERMINATION OF HEAT TRANSFER

The fringe patterns (for example Figs. 3 and 8) were magnified using a Vickers projection microscope, and in general this gave a substantial number of near-wall fringes, especially for the smooth wall, and for lower Re (see Fig. 4 of ref [12]) The fringes were then numbered and temperatures attached to each fringe according to equation (1) Three alternative situations were possible depending on whether

(i) a reasonable number of fringes were in the viscous sublayer with wall shear-stress data,

(ii) the nearest fringes were in the fully turbulent region, wall shear-stress data being available, or

(iii) as (ii) but with no wall shear-stress data

Method (i)

In this case, the wall heat flux is given by $q_w = \mathrm{d}T/\mathrm{d}y$, and T_w is given by an extrapolation formula In the example given by Lockett [25] for a smooth wall at $Re = 9800$, q_w and T_w were calculated as 275 W m^{-2} and 326 41 K, respectively, giving a value of $Nu = 35\ 5$ This compared with 31 4 calculated from

$$Nu = 0\ 023 Re^{0\cdot 8} Pr^{0\cdot 4} \qquad \text{(A1)}$$

Also using the wall shear-stress data the fringe temperatures and positions could be transformed into the non-dimensional $T^+ - y^+$ relationship

Method (ii)

Where the near wall fringes were all in the turbulent region, the wall temperature could be found by extrapolation, knowing the y^+ values for each fringe from the wall shear-stress data Use of the temperature log-law is also necessary This was the case with the square-rib geometry, where wall shear-stress data obtained by Mile at Harwell using Laser Doppler Anemometry [26] was taken

Method (iii)

Where no wall shear-stress data are available, as with the rounded-rib geometry, it is still possible to calculate the local q values from the fringe temperature gradients However only the relative, not the absolute, heat transfer values can be determined

To make this a totally self-contained method, therefore, accurate knowledge of the local wall shear-stress variation is needed

INTERFEROMETRIE HOLOGRAPHIQUE APPLIQUEE AU TRANSFERT THERMIQUE EN ECOULEMENT TURBULENT SUR DES RUGOSITES

Résumé—La méthode non intrusive de l'interférométrie holographique est appliquée au probleme du transfert thermique en écoulement turbulent sur des éléments de rugosité par nervures carrées et arrondies On montre que pour des isothermes bidimensionnelles cette méthode fournit des résultats locaux sur le transfert thermique Les données sont comparées avec celles d'autres méthodes expérimentales Bien que la géométrie simule spécifiquement celle d'un élément combustible de réacteur nucléaire refroidi par gaz, les resultats sont d'interêt genéral parce que le rapport pas sur hauteur des nervures est de 7,2 1

DIE ANWENDUNG DER HOLOGRAFISCHEN INTERFEROMETRIE ZUR UNTERSUCHUNG DES WÄRMEÜBERGANGS AN RIPPENRAUHIGKEITEN IN TURBULENTER STRÖMUNG

Zusammenfassung—Die nicht-invasive optische Methode der holografischen Interferometrie wird auf den Wärmeubergang in turbulenter Stromung über quadratische und rundliche Rippenelemente angewandt Neben der Darstellung zweidimensionaler Isothermen im Fluid wird gezeigt, daß diese Methode zuverlassige Daten fur den ortlichen Warmeubergang an der Oberflache liefert Diese Daten werden mit solchen aus anderen experimentellen Untersuchungen verglichen Die geometrische Anordnung entspricht zwar derjenigen bei fortschrittlichen Brennelementen eines gasgekühlten Reaktors, die Ergebnisse sind hingegen von allgemeinem Interesse, da das Verhaltnis von Rippenabstand zu Rippenhohe 7,2 1 betragt

ПРИМЕНЕНИЕ ГОЛОГРАФИЧЕСКОЙ ИНТЕРФЕРОМЕТРИИ К ТЕПЛОПЕРЕНОСУ ПРИ ТУРБУЛЕНТНОМ ТЕЧЕНИИ НАД РЕБРИСТЫМИ ШЕРОХОВАТОСТЯМИ

Аннотация—Оптический метод голографической интерферометрии применяется к задаче теплопереноса при турбулентном течении на поверхности с квадратными и закругленными ребристыми элементами шероховатости. Помимо двумерных изотерм данный метод позволяет получить надежные данные локального теплопереноса у поверхности. Эти данные сравниваются с результатами, полученными альтернативными экспериментальными методами В связи с тем, что геометрия элементов шероховатости моделирует геометрию топливных элементов усовершенствованного реактора с газовым охлаждением, полученные результаты представляют интерес